Dalton
www.rsc.org/dalton

Manganese complexes of mixed O, X, O-donor ligands (X = S or Se): synthesis, characterization and catalytic reactivity †

Tapan Kanti Paine, Thomas Weyhermüller, Eberhard Bothe, Karl Wieghardt and Phalguni Chaudhuri *

Max-Planck-Institut für Bioanorganische Chemie (formerly MPI für Strahlenchemie), Stiftstrasse 34-36, D-45470 Mülheim an der Ruhr, Germany.
E-mail: chaudh@mpi-muelheim.mpg.de

Received 29th April 2003, Accepted 19th June 2003
First published as an Advance Article on the web 4th July 2003

Complexes of manganese with two tridentate ligands, H_2L^{Se} and H_2L^{S}, containing [O, Se, O] or [O, S, O]-donor atoms, respectively, are described. The bisphenolate ligands yield complexes $[Mn^{III}{}_2L^{Se}{}_2(\mu\text{-}OCH_3)_2(CH_3OH)_2]$ **1**, $[Mn^{III}{}_2L^{S}{}_2(\mu\text{-}OCH_3)_2(CH_3OH)_2]$ **2**, $Bu_4N[Mn^{III}L^{Se}{}_2]$ **3**, $Bu_4N[Mn^{III}L^{S}{}_2]$ **4**, $[Mn^{IV}L^{Se}{}_2]$ **5** and $[Mn^{IV}L^{S}{}_2]$ **6**. The ferrocene adduct of **5**, *i.e.* $[Mn^{IV}L^{Se}{}_2]\cdot Fe(C_5H_5)_2$ **5a** is also described. The crystal structures of **1**, **5a** and **6** have been determined. The compounds have been thoroughly characterized by various physical methods, including IR, MS, UV-vis, EPR and magnetic susceptibility measurements. Low temperature electrochemical results at −25 °C strongly suggest that the electrochemical oxidations are not only ligand-centered, *i.e.* formation of phenoxyl radicals from the coordinated phenolates, but also metal-centered generating Mn(IV) species. The manganese(III) monomers **3** and **4** have been found to be oxidation catalysts with dihydrogen peroxide as the oxidant for epoxidation of alkenes, like styrene, stilbene and cyclohexene. The selenium containing ligand exhibits higher turnover numbers than the sulfur containing ligand.

Introduction

Manganese is present at the active site of a wide range of enzymes and participates in a variety of biological reactions.[1] Some of these enzymes, *e.g.* catalases, ribonucleotides reductase, oxygen evolving PSII, contain active sites composed of two or more metal ions. A tetranuclear manganese cluster at the heart of PSII has been observed by a structural characterization at a 3.8 Å resolution; in this dangler model one manganese ion is distinct from the other three.[2] This has attracted the attention to both triangular manganese and mononuclear Mn(IV) complexes and inspired study of manganese complexes as structural and functional models for the enzymes. Some of these model manganese complexes have been used in oxidation reactions of organic substrates with oxidants such as *tert*-butyl hydroperoxide, sodium hypochlorite or iodosylbenzene.[3] These reagents are expensive and hazardous and hence environmentally benign and cheaper oxidants like molecular oxygen or hydrogen peroxide are warranted. Hydrogen peroxide has already been used as oxidant with manganese complexes of various ligands.[4]

Phenol containing ligands[5,6] have attracted considerable attention in the coordination chemistry because of widespread occurrence of tyrosyl radicals[7] in a variety of metalloenzymes involved in oxygen-dependent enzymatic catalysis. An interesting feature associated with the ligands containing two phenolate donor atoms is their good π-donor ability to stabilize higher oxidation states with highly covalent M–O(phenolate) bonds and their tendency to form phenoxyl radical complexes.

In our continuing research using tridentate bisphenol ligands[6] for generating novel transition metal complexes with catalytic activities, we report here two μ-dimethoxo dimanganese(III) complexes and their aerial oxidation to mononuclear Mn(IV) complexes of bisphenol ligands with O, X, O donor sets (X = S, Se). We also wish to report two manganese(III) complexes $Bu_4N[Mn^{III}L^{X}{}_2]$ (X = S, Se), their structural, spectroscopic, electrochemical properties, and their use as catalysts for oxidation of alkenes with dihydrogen peroxide as the oxidant. The ligands used in this work are shown below:

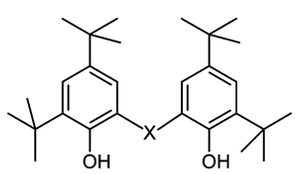

X = Se, $\mathbf{H_2L^{Se}}$;

X = S, $\mathbf{H_2L^{S}}$

Results and discussion

Synthesis and characterisation

Reaction of manganese salts and ligands in a suitable ratio afforded complexes **1**–**6** in relatively high yield (Scheme 1). Both the selenium and sulfur-containing bisphenolate ligands react with $MnCl_2\cdot 4H_2O$ in basic methanol to form bis(μ-methoxo)-dimanganese(III) complexes, **1** and **2**, respectively. A CH_3OH molecule occupies the sixth coordination sphere of each manganese center making them relatively reactive in aprotic or non-coordinating solvents. In CH_2Cl_2 **1** and **2** are easily oxidized by air to the mononuclear bisligand $[Mn^{IV}L_2]$ complexes **5** and **6**,

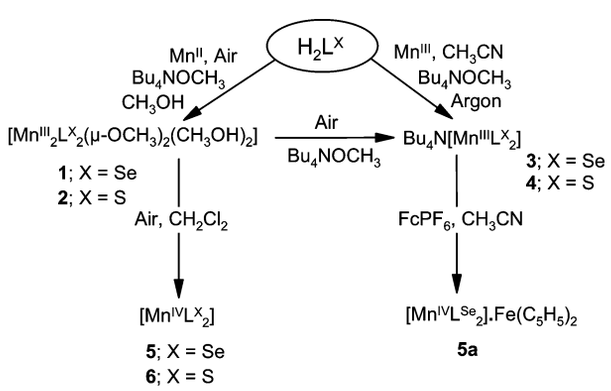

Scheme 1

† Electronic supplementary information (ESI) available: Fig. S1 and S2, plots of the magnetic susceptibility measurements – the experimental data with the simulations. See http://www.rsc.org/suppdata/dt/b3/b304765m/

DOI: 10.1039/b304765m

with concomitant formation of MnO_2. The ligands H_2L^X (X = S, Se) react with "Mn(III) acetate" in CH_3CN with Bu_4NOCH_3 or Bu_4NOH as bases to form complexes **3** and **4**, $Bu_4N[Mn^{III}L^X_2]$. Treatment of the bis(μ-methoxo) dimers **1** and **2** with Bu_4NOCH_3 also yields same complexes **3** and **4**. Chemical oxidation of complex **3** by $FcPF_6$ affords the mononuclear Mn(IV) complex $[Mn^{IV}L^{Se}_2]\cdot Fe(C_5H_5)_2$, **5a** in high yield.

IR data for the complexes are given in the Experimental section. The presence of the ligands was confirmed by a strong peak in the region 3000–2800 cm^{-1} due to ν(C–H) of *tert*-butyl groups of the ligands together with the other ν(C–H, C=C, C–O) vibrations found in the normal range for these types of linkages. The bands due to ν(OH) for the free ligands are replaced by a broad peak in the region 3200–3400 cm^{-1} after complexation, indicating the loss of phenol character of the ligand. The broad band at 3442/3 cm^{-1} for **1** and **2** is indicative of an alcohol. A weak but sharp peak at around 1050 cm^{-1} present in **1** and **2** is absent in the IR spectra of mononuclear complexes, indicating presumably coordinated methanol.

Except for μ-methoxo complexes, **1** and **2**, mass spectrometry in the EI and ESI modes has proved to be a very useful analytical tool for the characterization of the complexes and also for the identification of the metal center, and the compositions are in good agreement with the elemental analysis. EI-mass spectrometry for the μ-methoxo complexes **1** and **2** does not provide much information. But in the EI-mass spectrum for **6** the parent ion peak with 100% abundance is observed at m/z = 935 with the expected isotope pattern, confirming the composition $[Mn^{IV}L^S_2]$. Unfortunately, its selenium-congener does not provide such easily interpretable MS in the EI mode.

Mass spectrometry in ESI mode for **3** and **4** is in full conform with their mononuclear compositions. Two single peaks, one at m/z = 242.2 (in positive mode) and the second at m/z = 1031.6 or 935.5 (in negative mode) with the expected isotope distribution pattern, correspond to $[Bu_4N]^+$ and $[ML^{Se}_2]^-$, $[ML^S_2]^-$, species, respectively.

The optical spectra for complexes **1**–**6** have been measured in CH_2Cl_2 in the range 300–1000 nm. The bands are of charge-transfer origin, as is clear from their high absorption coefficient values. The peak at ~380 nm for **1** and **2** is of phenolate to Mn(III) charge-transfer origin. As it has already been pointed out, complexes **1** and **2** are susceptible to aerial oxidation in non-coordinating solvents. In CH_2Cl_2, the colour slowly changes from green to violet with the generation of a band around 530 nm (phenolate to Mn(IV) charge-transfer) and leaving a shoulder at the initial maximum at 380 nm range (Fig. 7a).

The UV-vis spectra of **3**–**6** exhibit ligand-to-metal charge transfer (LMCT) bands and π–π* transitions of the ligand. No d–d bands are observed due to the presence of strong long tails of the charge transfer bands at lower energy.

Single crystal X-ray diffraction studies

Complexes **1**, **5a**, and **6** were crystallographically characterized. The analytical, spectroscopic and magnetic data for **1** and **2** showed their isostructural character and hence X-ray analysis of only **1** was undertaken to remove the doubts regarding connectivity. As the characterization of isostructural complexes **3** and **4** were unambiguous from different physical measurements, we refrained from their single-crystal studies.

Molecular structure of 1

Crystal structure analysis reveals the complex to be dimeric in nature and **1** consists of two six coordinated Mn(III) ions with the formula $[Mn_2L^{Se}_2(\mu\text{-}OCH_3)_2(CH_3OH)_2]\cdot 0.5CH_3OH\cdot 0.5H_2O$. The ball and stick diagram along with the atom-labeling scheme is shown in Fig. 1; selected bond angles and bond lengths are given in Table 1.

Table 1 Selected bond distances (Å) and angles (deg) for $[Mn_2L^{Se}_2(\mu\text{-}OCH_3)_2(CH_3OH)_2]$ (**1**)

Mn(1)–O(1)	1.866(7)
Mn(1)–O(2)	1.856(6)
Mn(1)–O(30)	1.939(6)
Mn(1)–O(30)#1	1.956(6)
Mn(1)–O(40)	2.257(6)
Mn(1)–Se(1)	2.711(2)
C(1)–O(1)	1.340(10)
C(15)–O(2)	1.341(9)
O(2)–Mn(1)–O(1)	94.8(3)
O(2)–Mn(1)–O(30)	93.6(3)
O(1)–Mn(1)–O(30)	171.6(3)
O(2)–Mn(1)–O(30)#1	170.2(3)
O(1)–Mn(1)–O(30)#1	94.7(3)
O(30)–Mn(1)–O(30)#1	77.0(3)
O(2)–Mn(1)–O(40)	92.1(2)
O(1)–Mn(1)–O(40)	89.0(3)
O(30)–Mn(1)–O(40)	89.9(2)
O(30)#1–Mn(1)–O(40)	91.0(2)
O(2)–Mn(1)–Se(1)	82.9(2)
O(1)–Mn(1)–Se(1)	82.4(2)
O(30)–Mn(1)–Se(1)	99.5(2)
O(30)#1–Mn(1)–Se(1)	95.5(2)
O(40)–Mn(1)–Se(1)	168.6(2)
Mn(1)–O(30)–Mn(1)#1	102.5(3)
Mn(1) ··· Mn(1)#1	3.038(3)

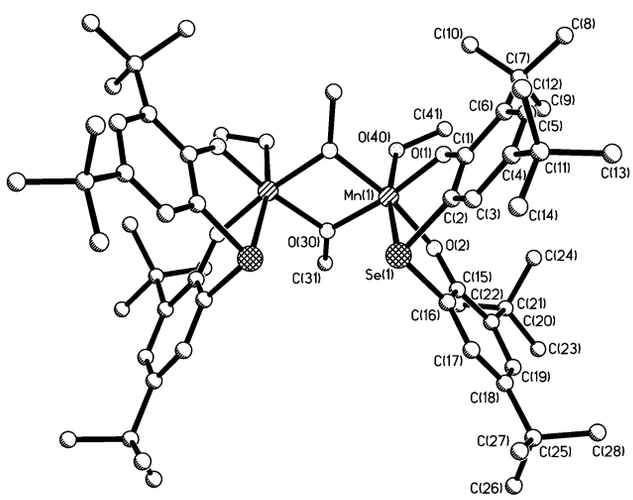

Fig. 1 Molecular structure of $[Mn_2L^{Se}_2(\mu\text{-}OCH_3)_2(CH_3OH)_2]$ **1**.

The two Mn(III) ions (Mn ··· Mn = 3.038 Å) are related by a crystallographic plane of symmetry and symmetrically bridged by two methoxide ligands. The bisphenolate ligand with an O,Se,O donor set is facially coordinated to the Mn(III) ions. Two bridging methoxy oxygens and two phenolate oxygens from ligands form the equatorial plane of the octahedral geometry for both Mn(III) centers. One selenium atom from the ligand and one oxygen atom from the methanol molecule occupying the *trans*-positions complete the coordination sphere. The selenium atoms from the ligands and the methanol molecules attached to two metal centers are *syn* to each other. Two manganese atoms and two bridging methoxy oxygens form a perfect plane, with Mn(1)–O(30)–Mn#(1) and O(30)–Mn(1)–O#(30) angles of 102.5 and 77°, respectively. The Mn(1)–Se(1) and Mn(1)–O(40) bonds form the axial plane with the O(40)–Mn(1)–Se(1) bond angle of 168.6°. The axial Mn(1)–O(40) bond distance with 2.257(6) Å is long presumably as a consequence of the Jahn–Teller elongation of the coordination polyhedron along the O(40)–Mn(1)–Se(1) direction and is in accord with the high spin d^4 electronic configuration of the Mn(III) centers. In contrast to the comparable dichromium(III) complexes reported earlier[6g] two methanol molecules are transposed although *syn* to each other, but no methanol/methanolate bridging is observed in **1**.

Table 2 Selected bond distances (Å) and angles (°) for $[MnL^{Se}_2]\cdot Fe(C_5H_5)_2\cdot CH_3CN$ (**5a**)

Mn(1)–O(1)	1.848(5)
Mn(1)–O(2)	1.866(5)
Mn(1)–O(3)	1.841(5)
Mn(1)–O(4)	1.876(5)
Mn(1)–Se(1)	2.4717(14)
Mn(1)–Se(2)	2.4848(14)
C(1)–O(1)	1.343(8)
C(15)–O(2)	1.321(9)
C(31)–O(3)	1.342(8)
C(45)–O(4)	1.332(8)
O(3)–Mn(1)–O(1)	93.2(2)
O(3)–Mn(1)–O(2)	92.0(2)
O(1)–Mn(1)–O(2)	93.9(2)
O(3)–Mn(1)–O(4)	94.0(2)
O(1)–Mn(1)–O(4)	91.5(2)
O(2)–Mn(1)–O(4)	171.7(2)
O(3)–Mn(1)–Se(1)	178.1(2)
O(1)–Mn(1)–Se(1)	86.4(2)
O(2)–Mn(1)–Se(1)	86.2(2)
O(4)–Mn(1)–Se(1)	87.9(2)
O(3)–Mn(1)–Se(2)	87.2(2)
O(1)–Mn(1)–Se(2)	177.0(2)
O(2)–Mn(1)–Se(2)	89.0(2)
O(4)–Mn(1)–Se(2)	85.6(2)
Se(1)–Mn(1)–Se(2)	93.36(5)

Molecular structure of 5a

The X-ray analysis confirms that the complex with M : L = 1 : 2 is formed. Fig. 2 shows the diagram of the independent molecule with the atom-labeling scheme. Selected bond distances and angles are given in Table 2.

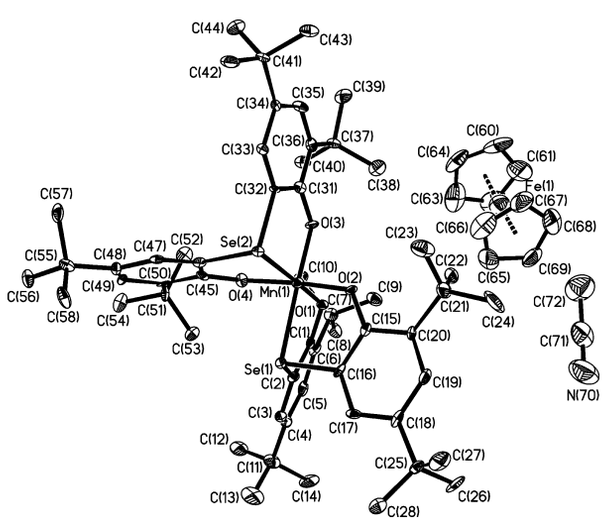

Fig. 2 A perspective view of the neutral complex **5a** $[MnL^{Se}_2]\cdot Fe(C_5H_5)_2\cdot CH_3CN$.

The complex consists of a neutral unit composed of a central pseudo-octahedral manganese ion surrounded by two tridentate ligands in a facial manner (*fac*-OSeO donor set). The complex is synthesized from its Mn(III) counterpart by chemical oxidation with $FcPF_6$ and the formed complex crystallizes with the reduced form of Fc^+, *i.e.* ferrocene, present in the solution. One solvent molecule, acetonitrile is also present in the unit cell. No π-interactions are prevailing between the ferrocene and the aromatic rings of the ligands (Fig. 2).

The ligands coordinate through the phenolate oxygens and selenium atoms. The phenols are deprotonated making the formal oxidation state of the central ion Mn(IV). The equatorial plane is composed of Se(1), Se(2), O(3) and O(1) atoms, in which the selenium or the oxygens donors are in *cis*-occupancy. The remaining phenolate oxygen atoms O(4) and O(2), mutually *trans*, complete the coordination sphere. The phenolate-containing bond lengths Mn(1)–O(3) and Mn(1)–O(1), which are disposed *trans* to Mn(1)–Se(1) and Mn(1)–Se(2), respectively, are significantly shorter with 1.845 Å than the remaining Mn(1)–O(4) and Mn(1)–O(2) with av. 1.871 Å, presumably due to *trans* influence. The bond angles O(2)–Mn(1)–O(4) [171.7(2)°], O(3)–Mn(1)–Se(1) [178.1(2)°], O(1)–Mn(1)–Se(2) [177.0(2)°], O(1)–Mn(1)–O(2) [93.9(2)°] and O(3)–Mn(1)–O(4) [94.0(2)°] clearly indicate the system to be a distorted octahedron. All the phenyl rings attached to the phenolate oxygen atoms are planar, indicating the retention of aromaticity of the phenyl rings. The mean Mn–O (phenolate) distance of 1.859 Å is consistent with other Mn(IV) complexes reported in the literature.[6f,8] The system is a genuine Mn(IV) and no ambiguity remains regarding the oxidation state of the metal, where the ligand is 'innocent' in this complex with metal in a higher oxidation state. The d^3 Mn(IV) electronic configuration corroborates also with the EPR and magnetic susceptibility measurements.

Table 3 Selected bond distances (Å) and angles (deg) for $[MnL^{S}_2]$ (**6**)

Mn(1)–O(1)	1.840(2)
Mn(1)–O(1)#1	1.840(2)
Mn(1)–O(2)	1.886(2)
Mn(1)–O(2)#1	1.886(2)
Mn(1)–S(1)	2.3586(8)
Mn(1)–S(1)#1	2.3586(8)
C(1)–O(1)	1.343(3)
C(15)–O(2)	1.346(3)
O(1)#1–Mn(1)–O(1)	90.91(11)
O(1)#1–Mn(1)–O(2)	92.29(8)
O(1)–Mn(1)–O(2)	96.57(8)
O(1)#1–Mn(1)–O(2)#1	96.58(8)
O(1)–Mn(1)–O(2)#1	92.29(8)
O(2)–Mn(1)–O(2)#1	167.36(12)
O(1)#1–Mn(1)–S(1)#1	85.92(6)
O(1)–Mn(1)–S(1)#1	175.96(6)
O(2)–Mn(1)–S(1)#1	86.06(6)
O(2)#1–Mn(1)–S(1)#1	85.60(6)
O(1)#1–Mn(1)–S(1)	175.96(6)
O(1)–Mn(1)–S(1)	85.92(6)
O(2)–Mn(1)–S(1)	85.60(6)
O(2)#1–Mn(1)–S(1)	86.06(6)
S(1)#1–Mn(1)–S(1)	97.35(4)

Molecular structure of 6

Complex **6** is the sulfur analogue of complex **5** and contains Mn(IV). As the structural properties of **5** and **6** are very similar details are not discussed here. The ORTEP diagram along with the atom-labeling scheme is shown in Fig. 3; selected bond angles and bond distances are listed in Table 3.

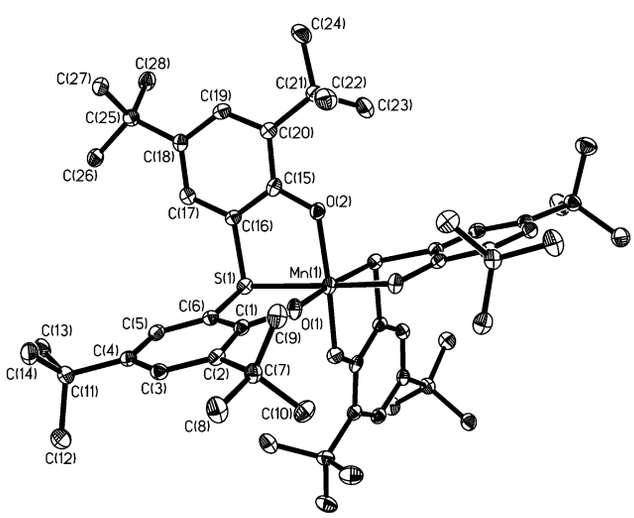

Fig. 3 An ORTEP representation of $[MnL^{S}_2]$ **6**.

Magnetic susceptibility measurements

Magnetic measurements for polycrystalline samples of complexes **1**–**6** were collected in the temperature range, 2–290 K in an applied field of 1 T. At 290 K the μ_{eff} values of 6.09μ_B ($\chi_M T$ = 4.64 cm^3 K mol^{-1}) for **1** and 6.42μ_B ($\chi_M T$ = 5.16 cm^3 K mol^{-1}) for **2** decrease monotonically with decreasing temperature until the μ_{eff} value of 0.52μ_B ($\chi_M T$ = 0.034 cm^3 K mol^{-1}) for **1** and 0.99μ_B ($\chi_M T$ = 0.12 cm^3 K mol^{-1}) for **2** at 2 K is attained; this is a clear indication of antiparallel exchange coupling between two paramagnetic Mn(III) centers (S_{Mn} = 2) with a resulting S_t = 0 ground state for both complexes **1** and **2**. Using the isotropic Heisenberg spin-Hamiltonian in the form $\hat{H} = -2J\,\hat{S}_1.\hat{S}_2$, the experimental magnetic data were simulated to evaluate the following best fit parameters: J = −11.8 cm^{-1}, g_{Mn} = 1.998 for **1** and J = −8.2 cm^{-1}, g_{Mn} = 1.998 for **2**. The experimental data with the simulations are provided as Fig. S1 and S2 (supplementary material†). The evaluated antiferromagnetic coupling constants between the high spin Mn(III) ions fall in the range observed for other μ-alkoxo dimanganese(III) complexes with comparable Mn ⋯ Mn distances.[9]

Above 15 K complexes **3** and **4** exhibit essentially temperature independent magnetic moments of μ_{eff} = 4.74 ± 0.03 for **3** and 4.86 ± 0.10 μ_B for **4**, confirming the high spin d^4 electronic configuration for the manganese centers. Simulations of the experimental magnetic data using S_{Mn} = 2.0, the zero-field splitting parameter D and g_{Mn}, yield g_{Mn} = 1.987, D = +2.9 cm^{-1} for **3** and g_{Mn} = 1.986, D = +3.4 cm^{-1} for **4** (Fig. S1 and S2, supplementary material†). We want to emphasize that the quality of fit decreases dramatically on changing the sign of D, thus indicating a positive zero-field splitting parameter for both **3** and **4**. We recall that too much significance should not be put on the sign and values of D evaluated through the fitting procedure of powder susceptibility data. We have confirmed the positive sign of the zero-field splitting parameters by performing temperature dependent magnetization measurements at different applied magnetic fields of 1, 4 and 7 T. Variable temperature-variable field magnetization measurements for **4** and their simulations are depicted in Fig. 4. The simulated parameters are S = 2.0 (fixed), g = 1.98 and D = +3.4 cm^{-1}.

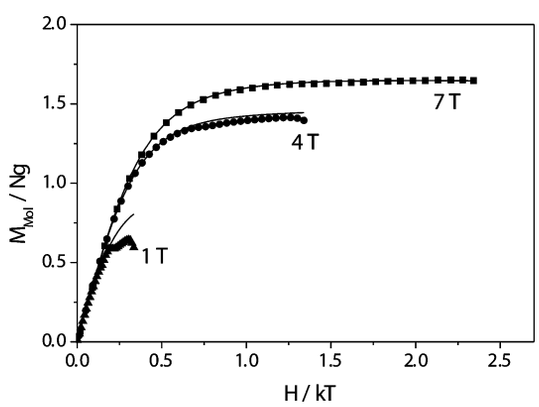

Fig. 4 The field-dependent magnetization of **4** as a function of temperature.

Above 10 K complexes **5a** and **5** show essentially temperature independent μ_{eff} values of 4.30 ± 0.10μ_B and 3.65 ± 0.03μ_B, respectively, thus corroborating with the d^3 electronic configuration for the manganese centers in these complexes. The higher μ_{eff} value for the Mn(IV) center in **5a** can be explained by the contribution of high TIP from ferrocene (low spin d^6) present in the crystals of **5a**. The magnetic moment of **6** is 3.83 ± 0.02μ_B, which is identical with the spin-only value for a d^3 system. Thus the experimental μ_{eff} values clearly indicate that we are dealing with genuine Mn(IV) species in **5**, **5a** and **6**.

Electrochemical studies

The electrochemical properties of the monomeric complexes **3**, **4**, **5** and **6** were investigated in CH_2Cl_2 solutions containing 0.1 M [(n-Bu)$_4$N]PF$_6$ as supporting electrolyte. A glassy carbon working electrode (2 mm disk; for higher scan rates a 0.25 mm Pt electrode was employed) and a Ag/AgNO$_3$ reference electrode was used. Ferrocene (Fc) was used as an internal standard and potentials are referenced *vs.* the ferrocenium/ ferrocene (Fc$^+$/Fc) couple.

The Mn^{III} and Mn^{IV} forms of the complexes (**3**, **4** and **5**, **6** respectively) can be electrochemically interconverted. The cyclic voltammograms of **3** and **5** and of **4** and **6** are identical and controlled potential coulometry of a solution of **3** at +0.3 V yields the UV-vis spectrum of **5** after a one-electron oxidation. The cyclic voltammograms belonging to such interconversion are shown for a slow scan rate (0.05 V s^{-1}) in Fig. 5a). Oxidative and re-reductive peaks are seen, but the separation of the peaks is about 0.3 V, *i.e.* much higher than that for an uncomplicated 1e$^-$ redox process (0.06 V). This high peak separation was found to depend strongly on the material of the working electrode (Pt and glassy carbon was used) and on the treatment of its surface (polishing procedure) prior to the measurements. This provides evidence that the high peak separation originates from a slow heterogeneous electron exchange rate rather than from interfering homogeneous reactions.

At higher scan rates (measured up to 30 V s^{-1}) (Fig. 5a) the cyclic voltammograms are more complex. When (with all complexes) the scan is started at positive potentials (*i.e.* the surrounding of the electrode consists after an equilibration time (15 s) only of the Mn^{IV} forms **5** or **6**), the reductive waves of **5** or **6** show at higher scan rates only the characteristics of slow electron transfer: peak broadening and a shift of the wave's maximum towards negative potentials. When, however, the scan is started at negative potentials, the reduction is the *second* process in the CV which takes place, depending on scan rate, only a short time after the preceding oxidation. In this case an additional reduction wave at more positive potentials grows in with increasing scan rate, at the expense of that for the "direct" reduction of Mn^{IV} to Mn^{III} seen at low scan rates. Clearly this extra peak must arise from a short-lived intermediate formed during the oxidation of **3** or **4**. At 30 V s^{-1} scan rate the wave for "direct" reduction has almost disappeared and the reduction takes place predominantly *via* this intermediate. It is noted that the oxidation appears at similar potentials as a single peak at all scan rates. This intermediate, which becomes visible at high scan rates because the "direct" metal-centered Mn^{III}/Mn^{IV} oxidation is kinetically hindered, must be formed *via* an alternative oxidation pathway of **3** or **4**. The only feasible alternative is a ligand-centered oxidation which generates a Mn^{III}–phenoxyl radical (Mn^{III}–O$^{\bullet}$) species. In the course of a slow scan it transforms into the thermodynamically slightly more stable Mn^{IV} which is re-reduced at potentials ≤ −0.3 V. At high scan rates, when the time required for a scan is shorter than the life time of the phenoxyl radical, only electrochemical reversible ligand-centered reduction at 0 V takes place.

The reaction scheme for the electrochemical **3/5** interconversion can be written as:

$$Mn^{III} - e^- \longrightarrow Mn^{IV},\ E^{0'} = -0.23\ V,\quad k_s = 5 \times 10^{-4}\ cm\ s^{-1},\ \alpha = 0.7 \qquad (1)$$

$$Mn^{III} - e^- \longrightarrow Mn^{III}\text{–}O^{\bullet},\ E^{0'} = -0.05\ V \qquad (2)$$

$$Mn^{III}\text{–}O^{\bullet} \longrightarrow Mn^{IV},\ k \approx 1\ s^{-1} \qquad (3)$$

where k_s is the heterogeneous rate constant, α is the transfer coefficient and k is the unimolecular rate constant of reaction (3).

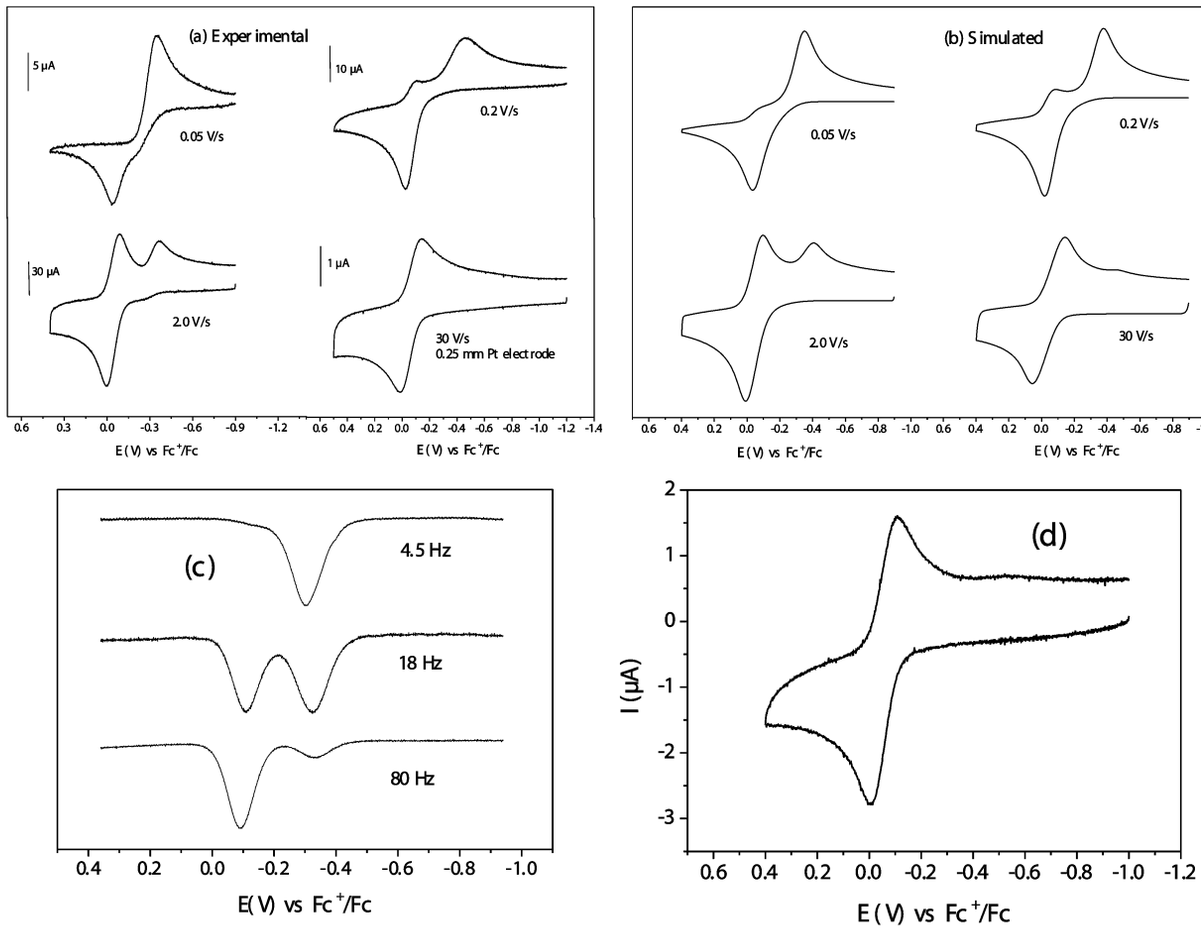

Fig. 5 Cyclic and square wave voltammograms (CV, SQW) of complex **3** in CH_2Cl_2 solution containing ~1 mM complex and 0.1 M $(n\text{-}Bu)_4NPF_6$. (a) Cyclic voltammograms of **3** in CH_2Cl_2 at room temperature with different scan rates. (b) Simulations of the cyclic voltammograms of **3** with different scan rates. (c) Square wave voltammograms of **3** in CH_2Cl_2 at room temperature with different scan frequencies. (d) Low-temperature cyclic voltammogram of **3** in CH_2Cl_2 at −25 °C.

The presence of two species and their approximate redox potentials can be observed even more clearly from the square wave voltammograms measured at different frequencies (range 4.5–80 Hz) in Fig. 5c.

With the system **3/5** we performed digital simulation and were able to reproduce the cyclic voltammograms of **3** at all scan rates using only eqn. (1)–(3) and the single set of parameters presented in the scheme. Examples are shown in Fig. 5b. This provides further evidence that the underlying reaction scheme of eqn. (1)–(3) is correct. It is noted however that the range of possible rate constants of eqn. (3) is 0.5–2.0 s^{-1} because the extent of transient Mn^{III}–$O^{\bullet}$ formation (and hence the appearance of the additional reductive peak at −0.06 V, the key fitting feature), is co-determined by the ratio of the contributions of the competing reactions (1) and (2). The contribution of (1), being a heterogeneous process, depends critically on the state of the working electrode's surface and could not be fully controlled.

The difference of the redox potentials of Mn^{IV}/Mn^{III} and Mn^{III}–$O^{\bullet}/Mn^{III}$ yields an equilibrium constant and a free energy change for the transformation of the phenoxyl radical of **3** into the Mn^{IV} species (eqn. (3)) of $K = 1.1 \times 10^3$ and $\Delta G^{\circ} = -17.4$ kJ mol^{-1}, respectively, at 25 °C ($\Delta E^{\mathbf{0}} = (RT/nF)$ ln K and $\Delta E^{\mathbf{0}} = -\Delta G^{0}/nF$)

At lower temperatures the rate constants of reactions (1) and (3) are expected to decrease, both with the consequence that less Mn^{IV} is present when it comes to re-reduction. Therefore at lower temperature $T = -25$ °C only the reversible Mn^{III}–$O^{\bullet}/Mn^{III}$ couple is observed as shown in Fig. 5d.

The system **4/6** shows very similar cyclic voltammograms, including the response to scan rate, and therefore the same mechanism is assumed to apply. The redox potentials are −0.22 V for the "direct" Mn^{IV}/Mn^{III} couple (measured with **6** and starting the CV at positive potentials) and +0.036 V for Mn^{III}–$O^{\bullet}/Mn^{III}$ (measured with **4** at high scan rates).

At higher potentials (≈+0.9 V with both, **3** or **4**) irreversible oxidation processes with high peak currents occur at slow scan rates in the cyclic voltammograms. They are most possible initiated by the oxidations of **3** or **4** to Mn^{IV}–$O^{\bullet}$ species.

EPR spectra

The EPR spectra of complexes **5** and **6** with simulations are given in Fig. 6 to show the signals observed for Mn(IV) complexes.

The complexity of EPR spectra for d^3 ions in an axial field ($E/D = 0$) is dependent upon the magnitude of the zero-field splitting parameters. The complexity can be reduced when either $2D \gg h\nu$ or $2D \ll h\nu$ ($h\nu = 0.31$ cm^{-1} for X-band EPR), where D is the axial zero-field splitting parameter. In the former case, two signals occur: a strong signal at low field and the a weaker $g = 2$ component, observed for Mn(IV)-catecholato and -sorbitolato complexes.[10] In the latter case, when D is small, the $g = 2$ signal dominates with weak low field signals, observed for Mn(IV)- thiohydroxamato[8c] and -thiocarbamato[11] complexes. The EPR spectra become isotropic when $D = 0$, exhibiting a strong signal in the $g = 2$ region.

Both complexes **5** in CH_2Cl_2 at 30 K and **6** in CH_2Cl_2/toluene cosolvent at 20 K show dominant signals at $g \approx 3$–6 and $g \approx 2$ with weakly resolved ^{55}Mn hyperfine lines ($I = 5/2$). The EPR spectra for both complexes are $S = 3/2$ powder pattern from

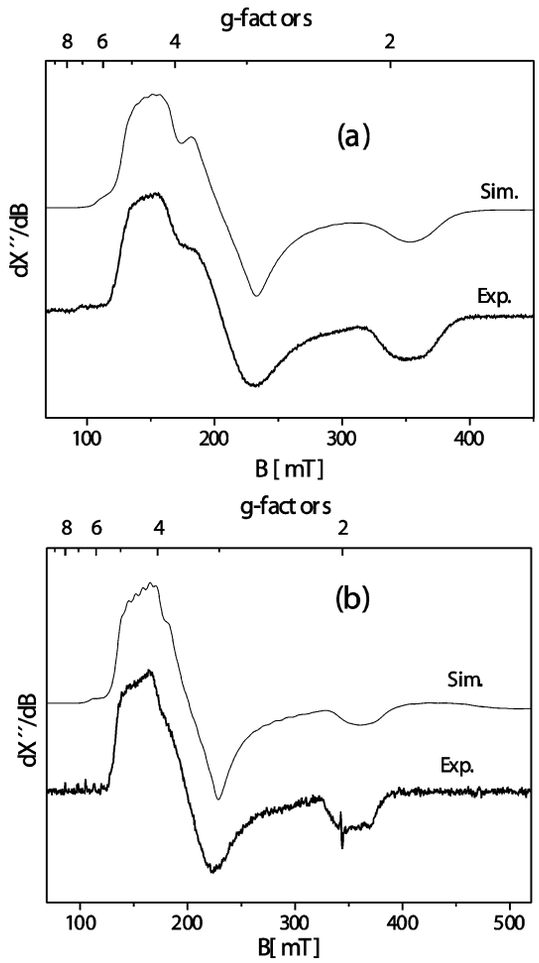

Fig. 6 X-band EPR spectra (a) for complex **5** in CH_2Cl_2 at 30 K and (b) for complex **6** in CH_2Cl_2/ toluene at 20 K. Experimental conditions (—): microwave frequency 9.45 GHz (**5**); 9.64 GHz (**6**), microwave power 0.1 mW (**5**); 0.2 mW (**6**), modulation amplitude 10 G (**5**); 10 G (**6**). The simulations (----): $g = 2.0$, $D = 0.56$ cm^{-1}, $E/D = 0.11$, $A = \{125, 140, 54\} \times 10^{-4}$ cm^{-1} for **5** and $g = 2.0$, $D = 0.47$ cm^{-1}, $E/D = 0.09$, $A = \{120, 140, 60\} \times 10^{-4}$ cm^{-1} for **6**; Lorentzian line with frequency-dependent line width $W = 670$ G (**5**); $W = 550$ G (**6**).

spin multiplets with moderately strong zero-field splitting (ZFS, $D \geq h\nu$). The signals at $g \approx 5$ and 3 can be assigned to powder resonance of the $|m_s = \pm 1/2>$ Kramer Doublets (KD) for fields along the molecular y- and x-directions, respectively. The trough at $g \approx 2$ originated from the z-resonances of $|m_s = \pm 1/2>$ KD. Significant population of the $|m_s = \pm 3/2>$ KD is indicated by the presence of low field hyperfine lines at $g \approx 6$, which also originated from fields in the z-direction.

Simulation of the experimental spectra yields the parameters, $D = 0.47$ cm^{-1}, $E/D = 0.09$ cm^{-1}, $g = 2.0$ and $A = (120, 140, 60) \times 10^{-4}$ cm^{-1} for **6** and $D = 0.56$ cm^{-1}, $E/D = 0.11$ cm^{-1}, $g = 2.0$ and $A = (125, 140, 54) \times 10^{-4}$ cm^{-1} for **5**. The positive ZFS ($D > 0$) clearly indicates the ground state properties $|\pm 1/2>$ resonances.

Reactivity studies

The Mn(III) dimers **1** and **2** form in the presence of air the corresponding Mn(IV) mononuclear complexes, **5** and **6**, whereas addition of base under argon generates the Mn(III) mononuclear complexes, **3** and **4**. The aerial oxidation to Mn(IV) monomer can be monitored spectrophotometrically, and the spectral change for the conversion of **1** into **5** is shown in Fig. 7a.

Formation of **5** from **1** (and also **6** from **2**) by aerial oxidation probably proceeds *via* metal–oxo or peroxo intermediate species. This is supported by the formation of solid MnO_2 as one of the products during this transformation.

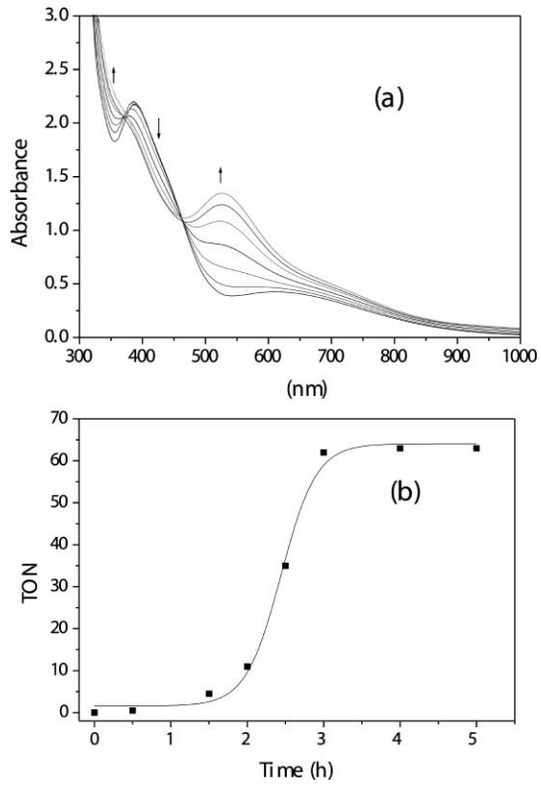

Fig. 7 (a) UV-vis spectral change of **1** in CH_2Cl_2 with time during the aerial oxidation to **5**. (b) Turnover numbers as a function of time for the oxidation of styrene to styrene oxide catalyzed by complex **3**.

These results and observations led us to study the reactivity of the complexes, *i.e.*, the oxidation reaction (epoxidation of alkenes). Unfortunately, air was found not to be an effective oxidant for the epoxidation of alkenes. But Mn(III)-monomers **3** and **4** are active oxidation catalysts with dihydrogen peroxide as the oxidant. *Complex* **3** was found to be a more efficient catalyst than the corresponding sulfur analogue **4** during the epoxidation reaction of styrene.

The catalytic oxidation reactions were carried out under standard conditions: 10^{-5} mol of the complex was dissolved with stirring in 10 ml CH_3CN at 0 °C. Subsequently, 10^{-2} mol of substrate alkenes, 10^{-3} mol of 2-methylimidazole and 10^{-2} mol of H_2O_2 were added ($t = 0$). After sometime, the solution became yellow when the sample was analysed and quantified using internal standards. The presence of the base is important for the oxidation process.

Oxidation of styrene

The major oxidation product observed in the GC from styrene is styrene oxide. The product was quantified after 4 h of reaction using undecane as an internal standard, yielding 69 turnovers with complex **3** and 51 turnovers with complex **4**. No other products were observed even after a long reaction time. The progress of the reaction, catalyzed by **3**, was monitored by GC and the resulting TON *vs.* time plot is shown in Fig. 7b. The sigmoidal nature of the reaction profile clearly indicates that initially (1.5–2 h) the reaction is very slow and then it becomes very fast. No further reaction takes place after 2.5 h. Presumably the reactive intermediate is formed slowly initially to react with the substrate yielding the oxidized product.

Oxidation of *cis*-stilbene

In the oxidation reactions of *cis*-stilbene catalyzed by complex **3**, isomerization occurs, resulting in both *cis*- (8 turnovers) and *trans*-epoxides (10 turnovers). *Trans*-stilbene (18 turnovers) is also observed in the reaction mixture.

Oxidation of cyclohexene

Oxidation of cyclohexene with complex **3** yields epoxide as a major product, with simultaneous formation of small amounts of cylohexenol and cyclohexenone (due to allylic oxidation). The products were quantified using undecane as an internal standard after 6 h. The oxidation of cyclohexene with **3** gave a turnover number of 42 towards the epoxide, and additionally the allylic oxidation products were formed with a turnover number of 11.

This oxidation of alkenes proceeds presumably *via* peroxide or hydroperoxide mechanism, formed *in situ* during the reaction of the Mn(III) complex and H_2O_2.

Concluding remarks

This paper has described ligating properties of two tridentate bisphenol ligands with either [O,S,O] or [O,Se,O] donor atoms towards the manganese center. Bis(homoleptic) complexes like $[Mn^{III}L_2]^-$ and $[Mn^{IV}L_2]^0$ together with bis-(methoxo)dimanganese(III) complexes have been isolated and thoroughly studied. X-ray structural studies have shown the facial coordination mode of the phenolate ligands. Electrochemical results suggest that the electrochemical oxidations are not only ligand-centered, *i.e.* formation of phenoxyl radicals from the coordinated phenolates, but also metal-centered generating Mn(IV) species. This latter oxidation occurs at such a low potential that the dimanganese(III) complexes are air-sensitive thus making isolation of Mn(IV) species easily viable.

A notable outcome from the epoxidation studies is the observation that the selenium-containing ligand leads to larger turnover numbers than the corresponding sulfur-containing ligands.

The realization that the present ligand system H_2L^X (X = S or Se) has the potential to generate easily oxidizable in air mono- and dinuclear complexes elicits the prospect of designing metal ligand systems which should have rich catalytic chemistry worthy of greater exploration.

Experimental

Syntheses

The ligand H_2L^S was synthesized according to a published procedure.[12] The ligand H_2L^{Se} was synthesized by a modified method.[13]

2,2′-Selenobis(4,6-di-*tert*-butylphenol) H_2L^{Se}. A suspension of 2,4-di-*tert*-butylphenol (61.89 g, 0.3 mol) and SeO_2 (11.1 g, 0.1 mol) in 55 ml conc. HCl was heated at 80 °C with constant stirring for 2 h. The mixture was then cooled, extracted with $CHCl_3$ (3 × 100 ml), washed with brine solution (2 × 50 ml) and then with water (100 ml), dried over Na_2SO_4 and concentrated *in vacuo*. The crude brown product was then recrystallized from heptane and CH_3OH (1 : 1) to obtain a pure white compound. Yield: 18.5 g (25%). Melting point: 141 °C. Anal. Calcd for $C_{28}H_{42}SeO_2$ (489.6 g mol^{-1}): C, 68.69; H, 8.65. Found: C, 68.7; H, 8.7%. ^{1}H-NMR ($CDCl_3$): δ 1.20 (s, 18H); 1.38 (s, 18H); 6.25 (s, OH, 2H); 7.24 (m, 4H). ^{13}C NMR ($CDCl_3$): δ 29.5 (s, *tert*-butyl); 31.6 (s, *tert*-butyl); 34.3 (s, *tert*-butyl); 35.2 (s, *tert*-butyl); 117.0 (s), 125.4 (s); 129.6 (s); 135.7(s); 143.3 (s), and 151.6 (s). MS (EI): the desired molecular ion (M^+ = 490) was observed in the ratio calculated for the naturally abundant isotope mixture of Se-74, 76, 77, 78, 80 and 82.

General method of synthesis for complexes 1 and 2

The ligand (1 mmol), dissolved in dry CH_3OH (25 ml) was treated with Bu_4NOCH_3 (2.5 ml) and stirred under argon for 5 min to yield a yellow solution, in which $MnCl_2{\cdot}4H_2O$ (0.19 g, 1 mmol) was added, and the resulting brown solution was refluxed under argon for 0.5 h. After cooling the solution was opened to air and stirred for another 15 min. A green microcrystalline compound was isolated, which was filtered and dried. X-ray quality crystals were grown from CH_2Cl_2/CH_3OH (1 : 1) cosolvent.

$[Mn_2L^{Se}_2(\mu\text{-}OCH_3)_2(CH_3OH)_2]$ (1). Yield: 0.52 g (86%). Anal. Calcd for $C_{60}H_{94}Se_2O_8Mn_2$ (1211.20 g mol^{-1}): C, 59.50; H, 7.82; Mn, 9.07. Found: C, 58.0; H, 8.2; Mn, 8.7%. IR (cm^{-1}): 3443 (br), 2958–2867 (s), 1431 (s), 1255 (s), 1051–1019, 834, 732, 555. Absorption spectrum (CH_2Cl_2); λ_{max}/nm (ε/M^{-1} cm^{-1}): 387(5940), 618(1160).

$[Mn_2L^{S}_2(\mu\text{-}OCH_3)_2(CH_3OH)_2]{\cdot}3\ CH_3OH$ (2). Yield: 0.48 g (78%). Anal. Calcd for $C_{63}H_{108}S_2O_{12}Mn_2$ (1231.54 g mol^{-1}): C, 61.44; H, 8.84; Mn, 8.92. Found: C, 62.3; H, 8.4; Mn, 8.9%. IR (cm^{-1}): 3442 (br), 2959–2869 (s), 1433 (s), 1283–1256 (s), 1048, 835, 743, 556. Absorption spectrum (CH_2Cl_2); λ_{max}/nm (ε/M^{-1} cm^{-1}): 386(5310); 444 (sh), 600(920).

General method of synthesis for complexes 3 and 4

1 mmol of ligand was dissolved in 30 ml CH_3CN. To that, Bu_4NOCH_3 (20% methanolic solution, 2 ml) was added and the resulting solution was stirred for 5 min under argon. To the resulting orange solution "$Mn(OAc)_3$" (0.13 g, 0.5 mmol) was added and the solution was stirred under argon for 1 h at room temperature. The deep red solution was then filtered to remove any insoluble impurities and the filtrate was kept under a slow sweep of argon. Within 2 d red needle like crystals were isolated.

$Bu_4N[MnL^{Se}_2]{\cdot}CH_3CN$ (3). Yield: 0.38 g (58%). Anal. Calcd for $C_{74}H_{119}Se_2O_4MnN_2$ (1313.63 g mol^{-1}): C, 67.66; H, 9.13; N, 2.13; Mn, 4.18. Found: C, 66.2; H, 8.9; N, 2.7; Mn, 4.1%. IR (cm^{-1}): 3441 (br), 2953–2872 (s), 1426 (s), 1298 (s), 1091, 833, 730, 536. Absorption spectrum (CH_2Cl_2); λ_{max}/nm (ε/M^{-1} cm^{-1}): 372(sh), 461(1790). MS (ESI in CH_2Cl_2): *m*/*z* 242.2 (positive, Bu_4N^+), *m*/*z* 1031.6 (negative, M^-).

$Bu_4N[MnL^{S}_2]{\cdot}CH_3CN$ (4). Yield: 0.32 g (54%). Anal. Calcd for $C_{74}H_{119}S_2O_4MnN_2$ (1219.83 g mol^{-1}): C, 72.86; H, 9.83; N, 2.30; S, 5.25; Mn, 4.50. Found: C, 72.6; H, 9.7; N, 2.4; S, 5.6; Mn, 4.6 %. IR (cm^{-1}): 3421 (br), 2960–2874 (s), 1429 (s), 1298 (s), 1102, 835, 741, 548. Absorption spectrum (CH_2Cl_2); λ_{max}/nm (ε/M^{-1} cm^{-1}): 372 (sh), 475(1100). MS (ESI in CH_2Cl_2): *m*/*z* 242.2 (positive, Bu_4N^+), *m*/*z* 935.5 (negative, M^-).

General method of synthesis for complexes 5 and 6

The Mn(III) dimer was dissolved in CH_2Cl_2(15 ml) and kept under air for 10 h, whereupon the colour of the solution changed from deep green to deep violet. The solution was then concentrated to half of its volume and kept for 1 h. A brown solid precipitated (MnO_2), which was filtered off. The violet filtrate was concentrated to 2 ml and 2 ml CH_3CN was added and the solution was kept in the refrigerator. Overnight keeping resulted in a brown crystalline complex.

$[MnL^2]$ (6). Yield: 0.11 g (88%). Anal. Calcd for $C_{56}H_{80}S_2O_4Mn$ (936.31 g mol^{-1}): C, 71.84; H, 8.61; S, 6.85; Mn, 5.87. Found: C, 73.1; H, 8.7; S, 6.8; Mn, 5.8%. IR (cm^{-1}): 3448 (br), 2955–2867 (s), 1432 (s), 1253 (s), 1096, 833, 740, 557. Absorption spectrum (CH_2Cl_2); λ_{max}/nm (ε/M^{-1} cm^{-1}): 394 (sh), 522(7650), 700 (sh). MS (EI): *m*/*z* = 935 [M^+, 100%].

$[MnL^{Se}_2]{\cdot}Fe(C_5H_5)_2{\cdot}CH_3CN$ (5a). The Mn(III) monomer **2** (65 mg, 0.05 mmol) was dissolved in CH_3CN (10 ml). To that 25 mg $FcPF_6$ (0.075 mmol) was added and the solution was stirred under argon at −20 °C for 2 h. The resulting deep violet solution was then filtered to remove any insoluble solid. The solution was then concentrated to half of its original volume and kept in the refrigerator. Within 3 h needle-shaped crystals

Table 4 Crystal data and structure refinement for **1**, **5a** and **6**

	1	**5a**	**6**
Empirical formula	$C_{60}H_{94}Mn_2Se_2O_8 \cdot 0.5CH_3OH \cdot 0.5H_2O$	$C_{56}H_{80}MnO_4Se_2 \cdot Fc \cdot CH_3CN$	$C_{56}H_{80}MnS_2O_4$
Formula weight	1236.18	1257.14	936.26
Temperature/K	100(2)	100(2)	100(2)
Crystal system	Monoclinic	Monoclinic	Orthorombic
Space group	*P*2/*n*, no. 13	*P*2(1)/*c*	*Pccn*, no. 56
a/Å	15.798(2)	24.410(3)	19.6760(12)
b/Å	11.2908(12)	15.052(2)	15.4393(8)
c/Å	18.644(2)	18.558(2)	17.8833(8)
β/°	102.75(2)	107.21(2)	
Volume/Å^3, *Z*	3243.6(6), 2	6513.3(14), 4	5432.7(5), 4
Density (calc.)/Mg m^{-3}	1.266	1.282	1.145
Absorption coeff./mm^{-1}	1.561	1.580	0.361
Reflections collected	19414	40492	39935
Independent reflect.	4239	8486	4781 [*R*(int)=0.1128]
Final R_1 indices [$I > 2\sigma(I)$]	0.0740	0.0554	0.0522
R_1 indices (all data)	0.1157	0.1306	0.0947

resulted which were filtered and dried. Yield: 32 mg (50%). Anal. Calcd for $C_{68}H_{93}Se_2O_4MnFeN$ (1257.14 g mol^{-1}): C, 64.97; H, 7.46; Mn, 4.37. Found: C, 64.8; H, 7.9; Mn, 4.9%. IR (cm^{-1}): 3446 (br), 2958–2867 (s), 1430 (s), 1253 (s), 1089, 833, 731, 554. Absorption spectrum (CH_2Cl_2); λ_{max}/nm (ε/M^{-1} cm^{-1}): 357 (sh), 8100; 532(7550), 700 (sh).

Catalytic oxidation of alkenes

Catalytic oxidation reactions were performed in dry CH_3CN. The alkene was taken in the solvent and treated with the manganese(III) complex and the base, 2-methyl-imidazole at 0 °C. To that solution H_2O_2 was added (t = 0) and stirred in a closed vessel. The solution changed its colour slowly to yellow and a brown solid separated when the solution attained room temperature. The solution was then analysed by GC and the products were quantified with respect to an internal standard.

The blank reactions simply in the presence of the ligands did not show any oxidation of the alkenes.

Physical measurements

Fourier transform infrared spectroscopy on KBr pellets was performed on a Perkin-Elmer 2000 FT-IR instrument. Solution electronic spectra were measured on a Perkin-Elmer Lambda 19 spectrophotometer. Mass spectra were recorded either in the EI or ESI (in CH_2Cl_2) mode with a Finnigan MAT 95 or 8200 spectrometer. Magnetic susceptibilities of the polycrystalline samples were recorded on a SQUID magnetometer (MPMS, Quantum Design) in the temperature range 2–290 K with an applied field of 1 T. The resulting volume magnetization from the sample had its diamagnetic contribution compensated and was recalculated as volume susceptibility. Diamagnetic contributions were estimated for each compound by using Pascal's constants. Cyclic voltammetry and coulometric experiments were performed using an EG&G potentiostat/galvanostat; simulation of CVs using DigiSim 3.0 software by Bioanalytical Systems. X-band EPR spectra were recorded on a Bruker ESP 300E spectrometer equipped with a helium flow cryostat (Oxford Instruments ESR 910), an NMR field probe (Bruker 035M), and a microwave frequency counter HP5352B. Spin-Hamiltonian simulations of the EPR spectra were performed either with a program that was developed from the routines of Gaffney and Silverstone [14] and that specifically makes use of the resonance-search procedure based on a Newton–Raphson algorithm as described therein. GC of the organic products during catalysis were performed on HP 6890 instruments using an RTX-5 Amine 13.5 S-63 column. GC-MS was performed using the above columns coupled with a HP 5973 mass spectrometer with mass selective detector. NMR spectra were measured using DRX 400 spectrometer.

X-ray crystallographic data collection and refinement of the structures

Single crystals of **1**, **5a**, **6** were coated with perfluoropolyether, picked up with glass fibers, and mounted on a Nonius Kappa-CCD diffractometer equipped with a cryogenic nitrogen cold stream operating at 100(2) K. Graphite monochromated Mo Kα radiation (λ = 0.71073 Å) was used. Intensity data were corrected for Lorentz and polarization effects. The intensity data set of **6** were corrected for absorption with use of the program Gaussian face-indexed, whereas those for **1** and **5a** were not corrected. The Siemens SHELXTL software package was used for solution, refinement, and artwork of the structure, and neutral atom scattering factors of the program were used.[15] All structures were solved and refined by direct methods and difference Fourier techniques. Non-hydrogen atoms were refined anisotropically except disordered parts in the structure of compound **1**, and hydrogen atoms were placed at calculated position and refined as riding atoms with isotropic displacement parameters.

Two t-butyl groups, the coordinated methanol molecule and the bridging methanolate anion in **1** were found to be disordered and a split atom model was introduced to account for this. Carbon atoms C(7)–C(10), C(12)–C(14) and C(31) and C(41) were splitted on two positions, isotropically refined. Corresponding carbon–carbon distances and O–C distances of the methanol and methanolate moieties were restrained to be equal within their errors using the SADI instruction in SHELXL97. A water and a methanol molecule of crystallization are also disordered on two positions due to the crystallographic 2-fold axis running through the $Mn_2(OMe)_2$-unit. The atom positions were isotropically refined and occupation factors of 0.25 were assigned to account for the low electron density giving in total the formulation $[Mn^{III}_2L^{Se}(\mu\text{-}OCH_3)_2(OHCH_3)_2] \cdot 0.5CH_3OH \cdot 0.5H_2O$.

Crystallographic data of the compounds are given in Table 4.

CCDC reference numbers 208392–208394.

See http://www.rsc.org/suppdata/dt/b3/b304765m/ for crystallographic data in CIF or other electronic format.

Acknowledgements

The skilful technical assistance of Mrs. H. Schucht, Mr. A. Göbel and Mrs. U. Westhoff is thankfully acknowledged. We are grateful to the German Research Council (DFG) for the financial support (Project: Priority Program Ch 111/2–2).

References

1 *Metal Ions in Biological Systems*, ed. A. Sigel and H. Sigel, Marcel-Dekker, New York, 2000, vol. 37.

2 A. Zouni, H. T. Witt, J. Kern, P. Fromme, N. Kraub, W. Saenger and P. Orth, *Nature*, 2001, **409**, 739.
3 T. Katsuki, in *Catalytic Asymmetric Synthesis*, ed. I. Ojima, Wiley-VCH, Weinheim, 2000, p. 287.
4 For example: (*a*) W. R. Sanderson, *Pure Appl. Chem.*, 2000, **72**, 1289; (*b*) D. E. De Vos and T. Bein, *J. Chem. Soc., Chem. Commun.*, 1996, 917; (*c*) C. Zondervan, R. Hage and B. L. Feringa, *J. Chem. Soc., Chem. Commun.*, 1997, 419; (*d*) M. Hoogenraad, K. Ramkisoensing, S. Gorter, W. L. Driessen, E. Bouwman, J. G. Haasnoot, J. Reedijk, T. Mahabiersing and F. Hartl, *Eur. J. Inorg. Chem.*, 2002, 377.
5 For example: (*a*) J. A. Halfen, B. A. Jazdzewski, S. Mahapatra, L. M. Berreau, E. C. Wilkinson, L. Que, Jr. and W. B. Tolman, *J. Am. Chem. Soc.*, 1997, **119**, 8217; (*b*) Y. Wang and T. D. P. Stack, *J. Am. Chem. Soc.*, 1996, **118**, 13097; (*c*) D. Zurita, I. Gautier-Luneau, S. Menage, J. L. Pierre and E. Saint-Aman, *J. Biol. Inorg. Chem.*, 1997, **2**, 46; (*d*) E. Bill, J. Müller, T. Weyhermüller and K. Wieghardt, *Inorg. Chem.*, 1999, **38**, 5795 and references therein; (*e*) M. A. Halcrow, L. M. Lindy Chia, X. Liu, E. J. L. McInnes, L. J. Yellowlees, F. E. Mabbs, I. J. Scowen, M. McPartlin and J. E. Davies, *J. Chem. Soc., Dalton Trans.*, 1999, 1753; (*f*) S. Itoh, S. Takayama, R. Arakawa, A. Furuta, M. Komatsu, A. Ishida, S. Takamuku and S. Fukuzumi, *Inorg. Chem.*, 1997, **36**, 1407; (*g*) K. Yamato, T. Inada, M. Doe, A. Ichimura, T. Takui, Y. Kojima, T. Kikunaga, S. Nakamura, N. Yanagihara, T. Onaka and S. Yano, *Bull. Chem. Soc. Jpn.*, 2000, **73**, 903; (*h*) Y. Shimazaki, S. Huth, A. Odani and O. Yamauchi, *Angew. Chem., Int. Ed.*, 2000, **112**, 1666; (*i*) M. Vaidyanathan and M. Palaniandavar, *Proc. Indian Acad. Sci. (Chem. Sci.)*, 2000, **112**, 223; (*j*) C. N. Verani, E. Bothe, D. Burdinski, T. Weyhermüller, U. Flörke and P. Chaudhuri, *Eur. J. Inorg. Chem.*, 2001, 2161.
6 (*a*) P. Chaudhuri, M. Hess, U. Flörke and K. Wieghardt, *Angew. Chem., Int. Ed.*, 1998, **110**, 2217; (*b*) P. Chaudhuri, M. Hess, T. Weyhermüller and K. Wieghardt, *Angew. Chem., Int. Ed.*, 1999, **38**, 1095; (*c*) P. Chaudhuri, M. Hess, J. Müller, K. Hildenbrand, E. Bill, T. Weyhermüller and K. Wieghardt, *J. Am. Chem. Soc.*, 1999, **121**, 9599; (*d*) R. Siefert, T. Weyhermüller and P. Chaudhuri, *J. Chem. Soc., Dalton Trans.*, 2000, 4656; (*e*) C. N. Verani, E. Bothe, D. Burdinski, T. Weyhermüller, U. Flörke and P. Chaudhuri, *Eur. J. Inorg. Chem.*, 2001, 2161; (*f*) T. Weyhermüller, T. K. Paine, E. Bothe, E. Bill and P. Chaudhuri, *Inorg. Chim. Acta*, 2002, **337**, 344; (*g*) T. K. Paine, T. Weyhermüller, K. Wieghardt and P. Chaudhuri, *Inorg. Chem.*, 2002, **41**, 6538; (*h*) S. Mukherjee, T. Weyhermüller, E. Bothe, K. Wieghardt and P. Chaudhuri, *Eur. J. Inorg. Chem.*, 2003, 863.
7 (*a*) *Chem. Rev.*, 1996, **96**, issue 7, ed. R. H. Holm and E. I. Solomon; (*b*) *Metal Ions in Biological Systems*, ed. H. Sigel and A. Sigel, Marcel-Dekker, New York, 1994, vol. 30; (*c*) G. T. Babcock, M. Espe, C. Hoganson, N. Lydakis-Simantiris, J. McCracken, W. Shi, S. Styring, C. Tommas and K. Warncke, *Acta Chem. Scand.*, 1997, **51**, 533; (*d*) M. M. Fontecave and J. J. Pierre, *Bull. Soc. Chim. Fr.*, 1996, **133**, 653; (*e*) D. P. Goldberg and S. J. Lippard, *Adv. Chem. Ser.*, 1995, **246**, 59; (*f*) J. Stubbe and W. A. van der Donk, *Chem. Rev.*, 1998, **98**, 705; (*g*) P. Chaudhuri and K. Wieghardt, *Progr. Inorg. Chem.*, ed. K. D. Karlin, 2002, **50**, 151.
8 (*a*) M. W. Lynch, D. N. Hendrickson, B. J. Fitzgerald and C. G. Pierpont, *J. Am. Chem. Soc.*, 1984, **106**, 2041; (*b*) J. R. Hartman, B. M. Foxman and S. R. Cooper, *Inorg. Chem.*, 1984, **23**, 1381; (*c*) S. Pal, P. Ghosh and A. Chakravorty, *Inorg. Chem.*, 1985, **24**, 3704; (*d*) R. O. C. Hart, S. G. Bott, J. L. Atwood and S. R. Cooper, *J. Chem. Soc., Chem. Commun.*, 1992, 895; (*e*) M. K. Chan and W. H. Armstrong, *Inorg. Chem.*, 1989, **28**, 3779; (*f*) P. S. Pavacik, J. C. Huffman and G. Christou, *J. Chem. Soc., Chem. Commun.*, 1986, 43; (*g*) S. K. Chandra, P. Basu, D. Ray, S. Pal and A. Chakravorty, *Inorg. Chem.*, 1990, **29**, 2423; (*h*) S. M. Saadeh, M. S. Lah and V. L. Pecoraro, *Inorg. Chem.*, 1991, **30**, 8; (*i*) M. Mikuriya, S. Shigematsu, K. Kawano, T. Tokii and H. Oshio, *Chem. Lett.*, 1990, 729; (*j*) B. Adam, E. Bill, E. Bothe, B. Goerdt, G. Haselhorst, K. Hildenbrand, A. Sokolowski, S. Steenken, T. Weyhermüller and K. Wieghardt, *Chem. Eur. J.*, 1997, **3**, 308; (*k*) D. P. Kessissoglou, W. M. Butler and V. L. Pecoraro, *J. Chem. Soc., Chem. Commun.*, 1986, 1253; (*l*) T. M. Rajendiran, J. W. Kampf and V. L. Pecoraro, *Inorg. Chim. Acta*, 2002, **339**, 497.
9 A. Gelasco, M. L. Kirk, J. W. Kampf and V. L. Pecoraro, *Inorg. Chem.*, 1997, **36**, 1829.
10 (*a*) K. D. Magers, C. G. Smith and D. T. Sawyer, *Inorg. Chem.*, 1980, **19**, 492; (*b*) D. T. Richens and D. T. Sawyer, *J. Am. Chem. Soc.*, 1979, **101**, 3681.
11 K. L Brown, R. M. Dolding, P. C. Healy, J. K. Jessop and W. C. Ten, *Aust. J. Chem.*, 1974, **27**, 2075.
12 S. D. Pastor, J. D. Spivack and L. P. Steinhuebel, *Heterocycl. Chem.*, 1984, **21**, 1285.
13 (*a*) T. Thompson, S. D. Pastor and G. Rihs, *Inorg. Chem.*, 1999, **38**, 4163; (*b*) T. K. Paine, T. Weyhermüller, E. Rentschler and P. Chaudhuri, *Eur. J. Inorg. Chem.*, in press.
14 B. J. Gaffney and H. J. Silverstone, in *EMR of Paramagnetic Molecules*, ed. L. J. Berliner and J. Reuben, Plenum Press, New York, 1993, vol. 13.
15 G. M. Sheldrick, SHELXL-97, Program for refinement of crystal structures, University of Göttingen, Germany, 1997; G. M. Sheldrick, SHELXS-97, Program for solution of crystal structures, University of Göttingen, Germany, 1997.